Engineering Transactions, **69**(3): 315–332, 2021, doi: 10.24423/EngTrans.1367.20210826
Polish Academy of Sciences • Institute of Fundamental Technological Research (IPPT PAN)
Université de Lorraine • Poznan University of Technology

Research Paper

Optimized Electroless Ni-Cu-P Coatings for Corrosion Protection of Steel Rebars from Pitting Attack of Chlorides

Arkadeb MUKHOPADHYAY[1)], Sarmila SAHOO[2)*]

[1)] *Department of Mechanical Engineering*
Birla Institute of Technology
Mesra, Ranchi – 835215, India

[2)] *Department of Civil Engineering*
Heritage Institute of Technology
Kolkata – 700107, India
*Corresponding Author e-mail: sarmila.sahoo@gmail.com

Structures, constructions and bridges in coastal areas are greatly affected by the corrosive attack of chlorides. This reduces their lifetime and leads to losses due to their maintenance. This study aims to improve the lifetime and corrosion-proof behavior of steel rebars in the saline environment (3.5% NaCl) by applying electroless Ni-Cu-P coatings with high corrosion resistance. Ni-Cu-P coating was deposited on Fe-600 steel rebars. The coating was deposited by varying bath condition parameters, such as concentration of nickel sulphate, sodium hypophosphite and copper sulphate. This led to a variation in Ni, P and Cu content, and finally, the optimal bath combination was obtained using the Taguchi-based grey relational analysis. For concentrations of 25, 10 and 0.3 g/l nickel sulphate, sodium hypophosphite and copper sulphate, enhanced corrosion resistance of the coated rebars could be achieved with -350 mV E_{corr} and 0.4 μA/cm^2 I_{corr}. At the same time, the bare rebars had E_{corr} of -653 mV and I_{corr} of 11.7 μA/cm^2.

Key words: electroless Ni-Cu-P coating; steel rebar; chloride attack; potentiodynamic polarization.

1. Introduction

One of the most common problems encountered in reinforced concrete structures is reduction of their strength and lifetime due to attack from chlorides species [1–3]. Aggressive attack of chloride ions leads to pitting of rebars, especially in the marine environment [4–6]. The presence of a passivating oxide layer leads to C-steel rebars embedded in concrete to become corrosion resistant in an alkaline environment (pH $>$ 3) [7]. Beyond a critical chloride concentration level,

the threshold value is exceeded and the passive oxide layer is damaged [8–10]. The presence of carbon dioxide in the atmosphere also decreases the pH [11]. Thus, the damage of steel rebars is accelerated in the coastal areas and marine environment due to the high accumulation of chloride species penetrating through the concrete pores [12].

Counteractive measures need to be undertaken to prevent corrosion of rebars. The attack of corrosion species may be inhibited by admixtures in concrete that induce self-healing characteristics [13–18]. Selecting a suitable steel grade also results in enhanced corrosion performance of the rebars. Austenitic grade stainless steel tends to remain passive in simulated seawater [19]. High chromium steels or chromium-modified steels have high corrosion resistance due to the formation of a compact and dense passivating layer when exposed to corrosive species [20]. Recent studies have explored the potential of surface-engineered rebars for protection against aggressive chloride ions [21]. Enamel-based coatings are quite popular candidates for long-term corrosion protection of rebars in a chloride environment [22–24]. Pure enamel coatings provide excellent corrosion resistance over a long-term period (244 days) in a chloride environment in comparison to double- or mixed-enamel coatings [25]. Due to the tendency of enamel coatings to get damaged during transportation, careful handling is necessary during hauling. Epoxy coatings, on the other hand, provide commendable corrosion resistance and good bond strength with mortar [26]. Electrochemical tests conducted for two years revealed no damage to steel rebars due to the epoxy coatings' low permeability to chloride infiltration [27]. The corrosion resistance of epoxy coatings was further enhanced by adding nano-fillers [28, 29]. Furthermore, it was seen that a double coating comprising epoxy as the outer layer and enamel as the inner layer could prevent delamination and provide 180% improvement in corrosion resistance compared to the individual candidates [30]. Galvanization was also observed to improve the corrosion resistance of reinforcement steel in chloride contamination due to passivation over a long-term period [31, 32].

Recent studies have explored the potential of metallic nickel-based binary and poly-alloy coatings for corrosion protection of rebars in chloride and sulphate attacks [33–35]. Electrochemical tests revealed that Ni-W-P and Ni-Cu-P ternary alloy coatings have nobler corrosion potential in 3.5% NaCl and 0.5 M H_2SO_4 [34, 35]. Ni-Cu-P coatings deposited by electroless method over Fe-600 grade rebars have shown excellent potential in shielding them from chloride and sulphate attacks. Hence, the present work aims at obtaining optimized electroless Ni-Cu-P coatings on Fe-600 grade steel with higher corrosion resistance to pitting chloride attacks. Metallic nickel and poly-alloy coatings may also be deposited by electroplating [36, 37]. However, electroless coatings have high adhesion to the substrate and deposit uniformity and intricate parts can be coated with ease [38]. Such deposit characteristics are beneficial for coating ribbed and

indented rebars. Ribs and indentations are provided on rebars to have a better bonding with concrete. Thus, it is desirable in such a case that the coatings would closely follow the substrate roughness, which may be achieved by the electroless method. Furthermore, electroless nickel treatment is an eco-friendly alternative to hazardous chromium plating [39].

The present work aims to obtain optimized Ni-Cu-P electroless coatings on Fe-600 grade rebars as a protective barrier for corrosion prevention. Optimized electroless Ni-Cu-P coatings were obtained by Taguchi's orthogonal array-based grey relational analysis with the source of nickel, phosphorus and copper as process parameters and potentiodynamic polarization parameters as responses. Electrochemical methods have been successfully used in the past [40] to evaluate the corrosion resistance of rebars, and hence potentiodynamic polarization test was also considered in the present work. Coating characteristics were also studied for the electroless Ni-Cu-P coated rebars to ensure proper deposition.

2. Methodology

The electroless method was used to deposit Ni-Cu-P coatings on Fe-600 grade steel rebars. These rebars conform to the Bureau of Indian Standards IS 1786:2008 and vary with the provisions laid down in ISO 6935-2:2007 [41] due to India's geographical factors and practices. Electroless Ni-Cu-P coatings were deposited on ground substrates (0.4 μm Ra) after proper specimen preparation. The detailed coating bath composition, deposition conditions and sample preparation steps are shown schematically in Fig. 1. The average coating thickness is within 25–30 μm [42]. The bath parameters such as concentration of nickel sulphate (source of nickel), sodium hypophosphite (reducing agent and source of phosphorus) and copper sulphate (source of copper) varied as shown in Table 1. The nominal diameter of the rebars was 20 mm with 2 mm thickness. The specimens were immersed in a 200 ml bath for three hours. A total of nine experimental baths were formulated based on the combinations given in Taguchi's L_9 orthogonal array (OA). This resulted in a noteworthy reduction in the number of experimental trials.

The corrosion resistance was measured from electrochemical tests, i.e., potentiodynamic polarization (PDP). A conventional three-electrode cell was used (GILL AC, ACM Instruments). Fifteen minutes of settling time were assigned for the open circuit potential (OCP) to get stabilized. The corrosive media was 3.5% NaCl for simulating the marine environment and accelerated chloride attack. The exposed surface area of bare and coated rebars to the electrolyte was 1 cm^2. This was the working electrode polarized at 1 mV/s in anodic and cathodic direction (± 250 mV *versus* OCP). The other two electrodes included a platinum rod auxiliary electrode (AE) and a saturated calomel reference elec-

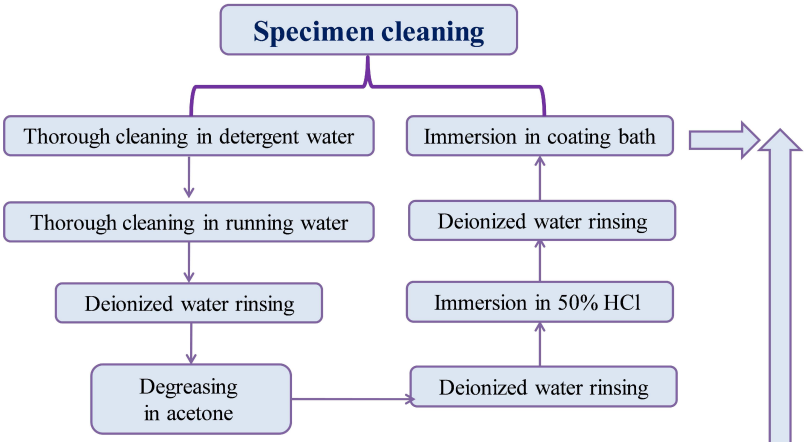

Chemical	Concentration [g/l]
Nickel sulphate	25–35
Sodium hypophosphite	10–20
Sodium citrate	15
Copper sulphate	0.3–0.7
Deposition Conditions	
pH	9.5
Bath volume	200 ml
Deposition temperature	85±2°C
Deposition duration	3 hours
Heat treatment	–
Agitation	–

FIG. 1. Schematic of specimen preparation and coating bath formulation.

Table 1. Concentrations of nickel, phosphorus and copper sources in the electroless bath.

Parameter levels	Concentrations [g/l]		
	Nickel sulphate (A)	Sodium hypophosphite (B)	Copper sulphate (C)
1	25	10	0.3
2	30*	15*	0.5*
3	35	20	0.7

* Initial combination of bath constituents.

trode (RE). The parameters of PDP tests were the corrosion current density (I_{corr}) and the corrosion potential (E_{corr}). These parameters were extrapolated from the Tafel polarization plots.

Based on the results of PDP, an optimization of corrosion resistance was carried out. A nobler E_{corr} and lower I_{corr} are desirable for enhanced corrosion performance. Thus, this formed the basis of a multivariate multi-objective optimization problem where the grey relational analysis (GRA) may be applied. The GRA is a very efficient and simple optimization technique that gives quick solution from discrete data points [43]. The GRA has been successfully used in optimizing multivariable problems in concrete compositions [44], various machining/micro-machining operations [45], friction and wear of electroless coatings [46], etc. The discrete data points (experimental combinations) and steps of the GRA are shown schematically in Fig. 2. The optimized results were compared with corrosion results of uncoated rebars.

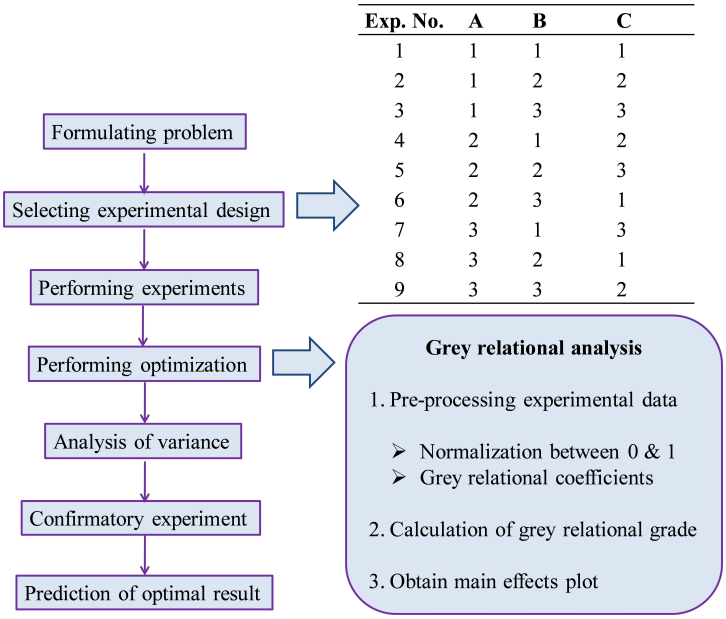

FIG. 2. Schematic of optimization problem formulation and solution using grey relational analysis.

Finally, coating characteristics such as composition, morphology and structure were addressed. A scanning electron microscope (SEM) was employed for studying surface morphology (JEOL, JSM 6390). For some specimens, field emission scanning electron microscope (FESEM) was also used (Sigma 300, Zeiss). Energy-dispersive X-ray spectroscopy (EDS) coupled with SEM was used to determine chemical compositions (EDAX Corporation and Oxford INCA). The coating structure was investigated with X-ray diffraction (XRD) at 1°/min scan rate for a range of 20–80° values of 2θ (Rigaku SmartLab). Some of the corroded specimens were also observed under SEM and FESEM.

3. Results and discussions

3.1. Optimized bath formulation and corrosion test results

Optimized coating bath constituents were obtained using the GRA. Nine PDP results obtained following the combinations as per Taguchi's OA (Fig. 2) for E_{corr} and I_{corr} are given in Table 2. Initially, the results need to be pre-processed in the GRA. Due to the different range of values and units of E_{corr} and I_{corr}, they are firstly normalized between 0 and 1. As a nobler E_{corr} is desired, it is normalized as per higher-the-better criteria. On the other hand, a lower corrosion current density indicates higher corrosion resistance. Hence, I_{corr} is normalized as per lower-the-better characteristics. Higher-the-better normalization is carried out as per the following formula [47]:

$$x_i^*(k) = \frac{x_i(k) - \min x_i(k)}{\max x_i(k) - \min x_i(k)}. \tag{3.1}$$

While lower-the-better is normalization is done as per the following formula [47]:

$$x_i^*(k) = \frac{\max x_i(k) - x_i(k)}{\max x_i(k) - \min x_i(k)}. \tag{3.2}$$

In Eqs (3.1) and (3.2), $\min x_i(k)$ and $\max x_i(k)$ are the smallest and largest values of $x_i(k)$, i.e., E_{corr} and I_{corr} given in Table 2.

Table 2. Results obtained from PDP tests and optimization.

Sl. No.	E_{corr} [mV]	I_{corr} [μA/cm^2]	Normalized values		Grey relational coefficient		Grade	Order	S/N ratio [dB]
			E_{corr}	I_{corr}	E_{corr}	I_{corr}			
1	−350	0.4	0.8093	1.0000	0.724	1.000	0.862	2	−1.29
2	−301	3.05	1.0000	0.8486	1.000	0.768	0.884	1	−1.07
3	−416	3.6	0.5525	0.8171	0.528	0.732	0.630	4	−4.01
4	−435	4.9	0.4786	0.7429	0.490	0.660	0.575	5	−4.81
5	−455	13.5	0.4008	0.2514	0.455	0.400	0.428	8	−7.38
6	−433	0.7	0.4864	0.9829	0.493	0.967	0.730	3	−2.73
7	−436	14.0	0.4747	0.2229	0.488	0.391	0.440	7	−7.14
8	−558	4.7	0.0000	0.7543	0.333	0.670	0.502	6	−5.99
9	−466	17.9	0.3580	0.0000	0.438	0.333	0.386	9	−8.28

Then, the grey relational coefficient (GRC) is calculated and the grey relational grade (GRG). The GRG is the multiple-performance indicator. The GRC is calculated as follows [47]:

$$\xi_i(k) = \frac{\Delta_{\min} + r\Delta_{\max}}{\Delta_{0i}(k) + r\Delta_{\max}}. \tag{3.3}$$

The GRC (ξ_i) for E_{corr} and I_{corr} are denoted as ξ_1 and ξ_2, respectively. The Δ value here, i.e., $\Delta_{0i} = \|x_{0i}(k) - x_i^*(k)\|$ whereas $\Delta_{\min}$ and $\Delta_{\max}$ is the minimum and maximum value respectively. The distinguishing coefficient (r) is 0.5 due to its moderate distinguishing ability [46, 47]. The deviation of the experimental data from the ideal best (which is 1) is denoted by the GRC. By combining the GRCs, the multi-performance index, i.e., the GRG is obtained. Average of ξ_1 and ξ_2 in a row gives the GRG. Finally, the quality loss function of Taguchi denoted by S/N ratio is calculated for maximization of the GRG since a higher value of the GRG (near to 1) would denote optimized condition. For higher-the-better criterion, it is given as [47]:

$$\text{S/N} = -10 \log \left(\frac{1}{n} \sum \frac{1}{y^2} \right). \tag{3.4}$$

Here y and n denote the observed data and total number of observations, respectively. The pre-processing, GRC, GRG and S/N ratios for all nine experimental runs are laid down in Table 2. Additionally, the order has been assigned to the GRG in Table 2. The highest value of the GRG is assigned order 1, while the lowest is assigned 9. The highest order resembles near optimum condition, whereas the lowest order signifies that the experimental result significantly deviates from the optimized condition.

In an OA, the effect of each process parameter may be determined at each level. This is done by finding out the mean S/N ratio of each process parameter at each level, and the results obtained are tabulated to form a 'response table of means'. The response table for means of S/N ratios in the present work is given in Table 3. Based on the delta values (difference between highest and lowest S/N ratio in a column), ranks have been assigned to the three process parameters: A, B and C denoting nickel sulphate, sodium hypophosphite and copper sulphate, respectively. Based on the ranks, the highest influence is observed for nickel sulphate, and hence rank 1 has been assigned, followed by copper sulphate and sodium hypophosphite. The optimal condition of parameters has been predicted

Table 3. Response table showing means of S/N ratios at different levels.

Level	A	B	C
1	−2.126	−4.412	−3.337
2	−4.973	−4.813	−4.719
3	−7.135	−5.008	−6.177
Delta	5.009	0.596	2.84
Rank	1	3	2
Mean S/N ratio = −4.74 dB			

from the main effects plot shown in Fig. 3. The optimized corrosion resistance of the Ni-Cu-P coated rebars has been achieved for a parametric combination of 25, 10, and 0.3 g/l nickel sulphate, sodium hypophosphite and copper sulphate respectively, i.e., $A_1B_1C_1$.

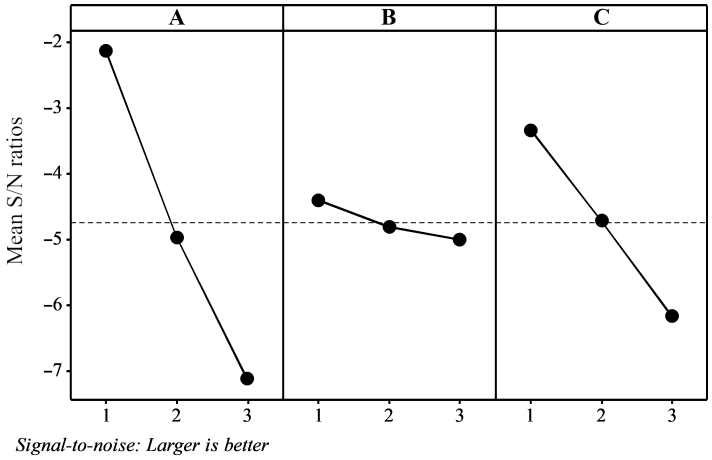

FIG. 3. Main effects plot showing means of S/N ratios.

Furthermore, analysis of variance (ANOVA) has been carried out on the S/N ratios given in Table 2. ANOVA is a very efficient statistical tool that gives the percent contribution of the factors on the multi-performance indicator, and the results are given in Table 4. From the ANOVA results given in Table 4, the highest significance in terms of the percentage contribution is for nickel sulphate (factor A) and copper sulphate (factor C). Thus, the concentration of nickel and copper in the bath has the highest influence in controlling the corrosion resistance of the coated rebars. The probability plot of S/N ratios is shown in Fig. 4 and it shows the adequacy of the model at a 95% confidence interval.

Table 4. ANOVA results for S/N ratios of GRG.

Source	DOF	Adjusted sum of squares	Adjusted mean squares	F-value	Percent contribution
A	2	37.87	18.94	6.14	66.80
B	2	0.55	0.28	0.09	0.98
C	2	12.10	6.05	1.96	21.35
Error	2	6.17	3.08		10.88
Total	8	56.70			100.00
R-sq = 89.12%					

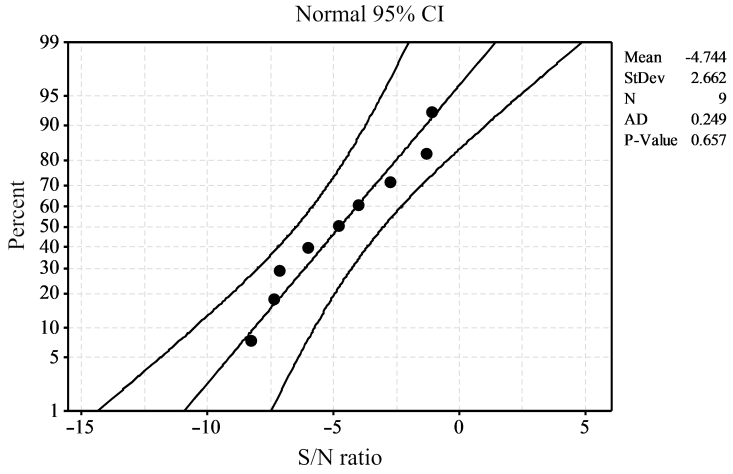

FIG. 4. Probability plot of S/N ratios showing the adequacy of the model.

Finally, a confirmation test has been carried out to conclude the suitability of the optimization. The optimal results are compared to an initial test run which is the combination of mid-level parameters in this case, $A_2B_2C_2$. The mid-level combination of parameters is selected based on a previous research work [34] where it was concluded that electroless Ni-Cu-P coatings could improve the corrosion performance of steel rebars in 3.5% NaCl. The aim of the present work is to achieve even higher corrosion resistance. The formula for predicting the grade at optimal parametric combination is [47]:

$$\widehat{\gamma} = \gamma_m + \sum_{i=1}^{o} (\overline{\gamma}_i - \gamma_m). \tag{3.5}$$

The mean GRG is γ_m. The mean GRG at optimal levels is denoted as $\overline{\gamma}_i$, and o represents the number of design variables (i.e., 3 in the present work). The results of the confirmatory run are shown in Table 5. The predicted and experi-

Table 5. Confirmatory test of optimization.

	Initial	Optimal	
		Predicted	Experimental
Level	$A_2B_2C_2$	$A_1B_1C_1$	$A_1B_1C_1$
E_{corr} [mV]	−356		−350
I_{corr} [μA/cm^2]	0.780		0.400
Grade	0.829	0.91	0.862
Improvement in grade = 0.033 (3.98%)			

mental grades are seen to be in accordance with each other. An improvement of almost 4% in the GRG is observed compared to the initial test.

The Tafel polarization plots of bare and Ni-Cu-P coated rebars at mid-level and optimal condition of parameters are shown in Fig. 5. A comparison of the corrosion parameters is shown in Table 6. A significant reduction in I_{corr} and nobler E_{corr} could be achieved due to the application of electroless Ni-Cu-P coatings compared to bare rebars. While there is no significant change in the mid-level or optimal parametric combination, Fig. 5 shows that there is the initiation of passivation at the optimum condition. Thus, the optimal bath combinations provide barrier as well as passive protection to the rebars. This may prove to be beneficial in the long-term corrosion protection of rebars and would prove to be beneficial compared to the initial parametric combination. Future research work may be directed towards the long-term investigation of corrosion resistance of the coated rebars to chloride attack.

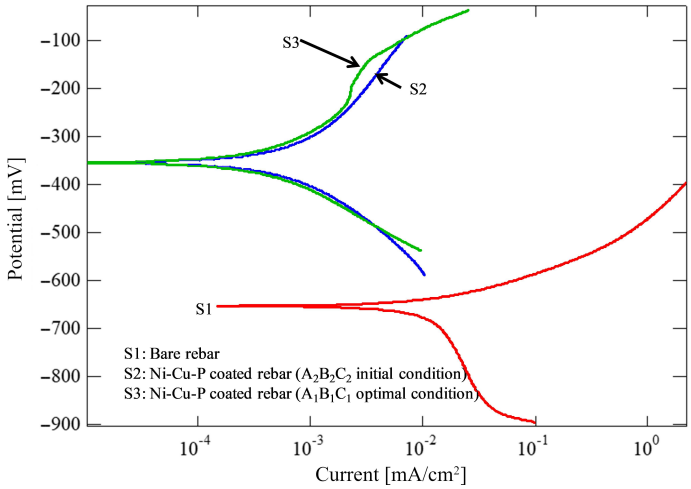

FIG. 5. Tafel plots of the bare and Ni-Cu-P coated rebars.

Table 6. Tafel polarization parameters of electroless coated and bare rebars.

Sl. No.	Corrosion parameters	Bare rebar	Ni-Cu-P coated rebars	
			Initial test run	Optimal condition
1	E_{corr} [mV]	−653	−356	−350
2	I_{corr} [μA/cm^2]	11.7	0.78	0.40

3.2. Study of coating characteristics

The surface morphologies observed in SEM and FESEM of Ni-Cu-P coated rebars for the initial test run and optimized bath formulation are shown in

Figs 6 and 7, respectively. For the former case, nodulated structures are observed (Fig. 6). The surface is dense and defect-free, i.e., without any porosities. This is the typical cauliflower-like morphology reported by other researchers, and the present observations are in line with them [33, 46]. In fact, a mass of round nodules was also observed for Ni-Cu-P coated magnesium by Liu *et al.* [48]. A compact mass of nodules is also seen in the optimized case in Fig. 7. The corresponding composition of the coated rebars is shown in Table 7, as they lie in the high phosphorus range leading to a high corrosion resistance. Ni-P electroless deposited coatings have proven corrosion resistant [49, 50] and this is enhanced on adding a third element because of their higher reduction potential compared to Ni [48]. It may also be noted here that Table 4 indicates the highest influence of nickel sulphate in controlling corrosion, which in turn controls the source

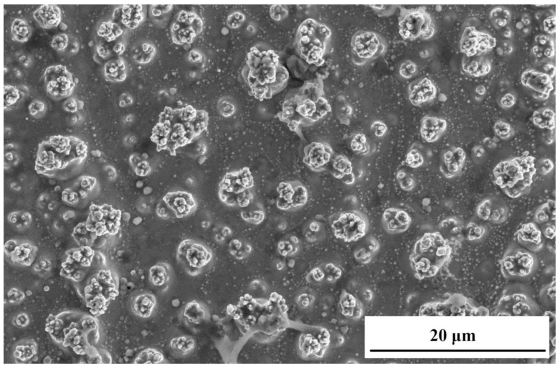

Fig. 6. SEM image of Ni-Cu-P coating deposited on Fe-600 grade rebar for initial combination of design variables at 2000X magnification (reproduced from [34] with permission from IOPscience).

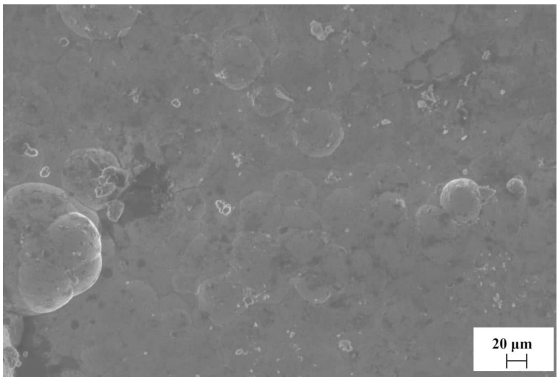

Fig. 7. FESEM image of Ni-Cu-P coating deposited on Fe-600 grade rebar for optimal combination of design variables at 5000X magnification.

of Ni. Thus, it is expected that the Ni content shown in Table 7 for both coated rebars is almost the same, leading to similar corrosion resistance. However, increasing Cu content in Ni-Cu-P coatings promotes passivation in the deposits when subjected to chloride attacks [48]. Here, in the optimized bath, the initiation of passivation is observed, which could be due to an optimal concentration of all the constituents in the electroless bath.

Table 7. EDS composition analysis of Ni-Cu-P coated rebars.

Combination	Wt.% of Ni	Wt.% of P	Wt.% of Cu
Initial	83–86	10–12	4–5
Optimal	85–88	9–11	3–4

The XRD results of coated rebars for initial and optimized combination are shown in Fig. 8. Both exhibit amorphous nature with a broad dome around $\sim 44^\circ$ 2θ. A sharp peak surrounded by a broad dome has also been referred to as a mixture of amorphous and nano-crystalline nature in other research works [51]. In the case of optimal condition (Fig. 8b), the strong peak at $\sim 45^\circ$ 2θ and the weaker peaks at $\sim 51^\circ$, 64°, and 73° for both initial and optimal conditions (Figs 8a and 8b) are from the substrate, i.e., intrinsic iron content [52]. In general, an increase in crystallinity has been observed with an increase in copper sulphate concentration and also an increase in corrosion resistance [48]. But in the present case, the coating crystallinity is correlated with the composition in Table 7, and they corroborate with each other. The results are also in agreement with other research works [48–52]. Thus, from the coating characteristics, effective coating deposition is concluded.

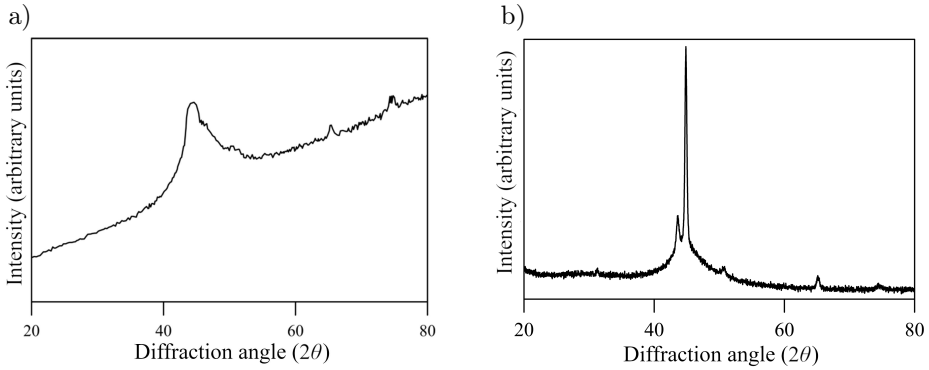

Fig. 8. Results of X-ray diffraction of electroless Ni-Cu-P coated rebars: a) initial combination (reproduced from [34] with permission from IOPscience) and b) optimized condition.

3.3. Study of corroded specimens

The bare rebar subjected to the chloride attack is shown in Fig. 9. The surface is characterized by severe cracking due to the pitting attack of the chloride species. The FESEM image of the optimized coated rebar post corrosion in 3.5% NaCl is shown in Fig. 10. The surface is comprised of passive products and lamellar structures. Similar structures have also been observed in the case of Ni-W-P coatings leading to enhanced corrosion resistance [47]. Thus, an optimized coating bath leads to a significant improvement in the corrosion performance of the rebars. Future research works may be directed towards the investigation of the long-term corrosion performance of the coated rebars in corrosive media since the present work reveals the onset of passivation. The present work

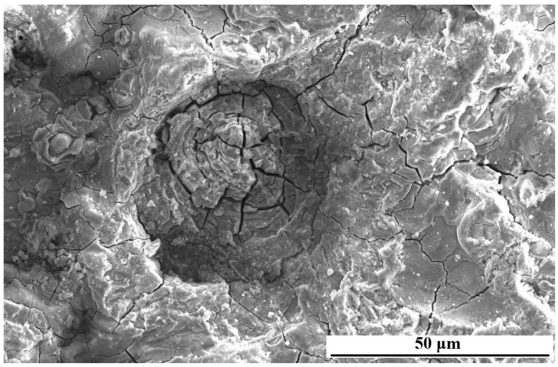

FIG. 9. SEM image showing chloride-induced corrosion in bare Fe-600 grade steel rebars at 1000X magnification (reproduced from [34] with permission from IOPscience).

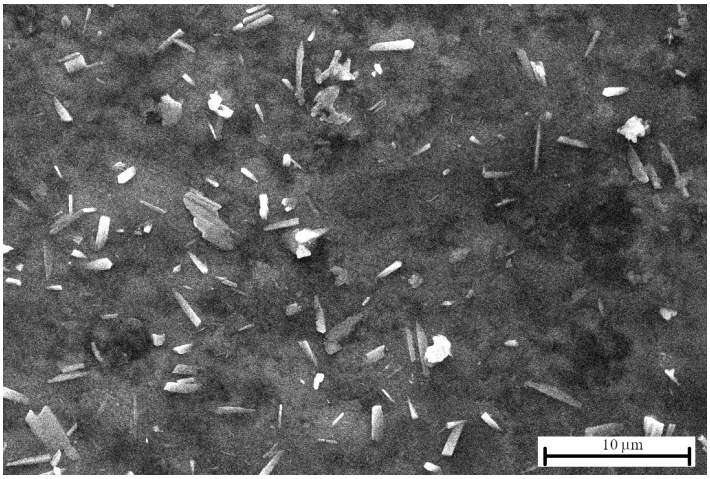

FIG. 10. FESEM image showing passivity in optimized Ni-Cu-P coated rebars after chloride-induced attacks at 6000X magnification.

would prove to be an initial step towards establishing electroless nickel coatings as suitable alternatives for corrosion protection of structures in saline/marine environment.

4. Conclusion

The present work investigated electroless Ni-Cu-P coatings as potential candidates for corrosion prevention of Fe-600 grade rebars in a chloride environment. To achieve enhanced corrosion resistance of the rebars, optimum coating bath formulation was predicted using the Taguchi-based grey relational analysis. A noble E_{corr} (-350 mV) and low I_{corr} (0.4 μA/cm^2) were achieved as a result of the optimization of the coating bath. On the other hand, the bare rebars had E_{corr} and I_{corr} of -653 mV and 11.7 μA/cm^2, respectively. The ANOVA results indicated a high influence of nickel sulphate concentration in the bath on controlling the corrosion resistance followed by copper sulphate concentration. PDP tests indicated the initiation of a passive film in the optimized coating, which could be advantageous for the long-term corrosion protection of the rebars. Coating characterization revealed a compact and defect-free deposition. This led to an efficient barrier as well as passive protection of the coated rebars in 3.5% NaCl. The Ni-Cu-P coatings were in the high phosphorus range. X-ray diffractions revealed the amorphous nature of the coated rebars. In post corrosion, the bare rebars showed severe cracking and spalling. On the other hand, corrosive products with lamellar structures were observed for the rebars coated in the optimized electroless bath. Thus, Ni-Cu-P coatings by the electroless method could be successfully applied in corrosion protection of reinforcement steel rebars. Future research works may be carried out to explore the long-term corrosion protection capacity of the deposits, effect of carbonation, graded nickel coatings, etc.

Acknowledgment

The authors gratefully acknowledge the coating characterization facility provided by the Central Instrumentation Facility (CIF) of Birla Institute of Technology, Mesra, Ranchi – 835215.

References

1. Song Y., Wightman E., Kulandaivelu J., Bu H., Wang Z., Yuan Z., Jiang G., Rebar corrosion and its interaction with concrete degradation in reinforced concrete sewers, *Water Research*, **182**: 115961, 2020, doi: 10.1016/j.watres.2020.115961.

2. Samson G., Deby F., Garciaz J.-L., Lassoued M., An alternative method to measure corrosion rate of reinforced concrete structures, *Cement and Concrete Composites*, **112**: 103672, 2020, doi: 10.1016/j.cemconcomp.2020.103672.

3. Cabrini M., Lorenzi S., Coffetti D., Coppola L., Pastore T., Inhibition effect of tartrate ions on the localized corrosion of steel in pore solution at different chloride concentrations, *Buildings*, **10**(6): 105, 2020, doi: 10.3390/buildings10060105.

4. Bolzoni F., Brenna A., Beretta S., Ormellese M., Diamanti M.V., Pedeferri M.P., Progresses in prevention of corrosion in concrete, *IOP Conference Series: Earth and Environmental Science*, **296**: 012016, 2019, https://doi.org/10.1088/1755-1315/296/1/012016.

5. Sadati S., Arezoumandi M., Shekarchi M., Long-term performance of concrete surface coatings in soil exposure of marine environments, *Construction and Building Materials*, **94**: 656–663, 2015, doi: 10.1016/j.conbuildmat.2015.07.094.

6. James A., Bazarchi E., Chiniforush A.A., Aghdam P.P., Hosseini M.R., Akbarnezhad A., Martek I. Ghodoosi F., Rebar corrosion detection, protection, and rehabilitation of reinforced concrete structures in coastal environments: A review, *Construction and Building Materials*, **224**: 1026–1039, 2019, doi: 10.1016/j.conbuildmat.2019.07.250.

7. Sagüés A.A., Pech-Canul M.A., Shahid Al-Mansur A.S., Corrosion macrocell behavior of reinforcing steel in partially submerged concrete columns, *Corrosion Science*, **45**(1): 7–32, 2003, doi: 10.1016/S0010-938X(02)00087-2.

8. Shi J., Ming J., Influence of defects at the steel-mortar interface on the corrosion behavior of steel, *Construction and Building Materials*, **136**: 118–125, 2017, doi: 10.1016/j.conbuildmat.2017.01.007.

9. Pradhan B., Bhattacharjee B., Rebar corrosion in chloride environment, *Construction and Building Materials*, **25**(5): 2565–2575, 2011, doi: 10.1016/j.conbuildmat.2010.11.099.

10. Manera M., Vennesland Ø., Bertolini L., Chloride threshold for rebar corrosion in concrete with addition of silica fume, *Corrosion Science*, **50**(2): 554–560, 2008, doi: 10.1016/j.corsci.2007.07.007.

11. Wang D., Ming J., Shi J., Enhanced corrosion resistance of rebar in carbonated concrete pore solutions by Na_2HPO_4 and benzotriazole, *Corrosion Science*, **174**: 108830, 2020, doi: 10.1016/j.corsci.2020.108830.

12. Wu M., Shi J., Beneficial and detrimental impacts of molybdate on corrosion resistance of steels in alkaline concrete pore solution with high chloride contamination, *Corrosion Science*, **183**: 109326, 2021, doi: 10.1016/j.corsci.2021.109326.

13. Kumar S., Yang E.-H., Unluer C., Investigation of chloride penetration in carbonated reactive magnesia cement mixes exposed to cyclic wetting–drying, *Construction and Building Materials*, **284**: 122837, 2021, doi: 10.1016/j.conbuildmat.2021.122837.

14. Cascudo O., Pires P., Carasek H., de Castro A., Lopes A., Evaluation of the pore solution of concretes with mineral additions subjected to 14 years of natural carbonation, *Cement and Concrete Composites*, **115**: 103858, 2021, doi: 10.1016/j.cemconcomp.2020.103858.

15. Liu S., Zhu M., Ding X., Ren Z., Zhao S., Zhao M., Dang J., High-durability concrete with supplementary cementitious admixtures used in corrosive environments, *Crystals*, **11**(2): 196, 2021, doi: 10.3390/cryst11020196.

16. Baltazar-Zamora M.A., M Bastidas D., Santiago-Hurtado G., Mendoza-Rangel J.M., Gaona-Tiburcio C., Bastidas J.M., Almeraya-Calderón F., Effect of silica fume and fly ash admixtures on the corrosion behavior of AISI 304 embedded in concrete exposed in 3.5% NaCl solution, *Materials*, **12**(23): 4007, 2019, doi: 10.3390/ma12234007.

17. Söylev T.A., Richardson M.G., Corrosion inhibitors for steel in concrete: State-of-the-art report, *Construction and Building Materials*, **22**(4): 609–622, 2008, doi: 10.1016/j.conbuildmat.2006.10.013.

18. Pan C., Chen N., He J., Liu S., Chen K., Wang P., Xu P., Effects of corrosion inhibitor and functional components on the electrochemical and mechanical properties of concrete subject to chloride environment, *Construction and Building Materials*, **260**: 119724, 2020, doi: 10.1016/j.conbuildmat.2020.119724.

19. Luo H., Su H., Dong C., Li X., Passivation and electrochemical behavior of 316L stainless steel in chlorinated simulated concrete pore solution, *Applied Surface Science*, **400**: 38–48, 2017, doi: 10.1016/j.apsusc.2016.12.180.

20. Tian Y., Liu M., Cheng X., Dong C., Wang G., Li X., Cr-modified low alloy steel reinforcement embedded in mortar for two years: Corrosion result of marine field test, *Cement and Concrete Composites*, **97**: 190–201, 2019, doi: 10.1016/j.cemconcomp.2018.12.019.

21. Mukhopadhyay A., Sahoo S., Corrosion protection of construction steel, [in:] Sahoo P. [Ed.], *Handbook of Research on Developments and Trends in Industrial and Materials Engineering*, pp. 327–347, 2020, IGI Global, doi: 10.4018/978-1-7998-1831-1.ch014.

22. Tang F., Chen G., Brow R.K., Volz J.S., Koenigstein M.L., Corrosion resistance and mechanism of steel rebar coated with three types of enamel, *Corrosion Science*, **59**: 157–168, 2012, doi: 10.1016/j.corsci.2012.02.024.

23. Tang F., Chen G., Volz J.S., Brow R.K., Koenigstein M.L., Microstructure and corrosion resistance of enamel coatings applied to smooth reinforcing steel, *Construction and Building Materials*, **35**: 376–384, 2012, doi: 10.1016/j.conbuildmat.2012.04.059.

24. Tang F., Cheng X., Chen G., Brow R.K., Volz J.S., Koenigstein M.L., Electrochemical behavior of enamel-coated carbon steel in simulated concrete pore water solution with various chloride concentrations, *Electrochimica Acta*, **92**: 36–46, 2013, doi: 10.1016/j.electacta.2012.12.125.

25. Tang F., Chen G., Brow R.K., Chloride-induced corrosion mechanism and rate of enamel- and epoxy-coated deformed steel bars embedded in mortar, *Cement and Concrete Research*, **82**: 58–73, 2016, doi: 10.1016/j.cemconres.2015.12.015.

26. Pour-Ali S., Dehghanian C., Kosari A., Corrosion protection of the reinforcing steels in chloride-laden concrete environment through epoxy/polyaniline–camphorsulfonate nanocomposite coating, *Corrosion Science*, **90**: 239–247, 2015, doi: 10.1016/j.corsci.2014.10.015.

27. Sohail M.G., Salih M., Al Nuaimi N., Kahraman R., Corrosion performance of mild steel and epoxy coated rebar in concrete under simulated harsh environment, *International Journal of Building Pathology and Adaptation*, **37**(5): 657–678, 2019, doi: 10.1108/IJBPA-12-2018-0099.

28. Rajitha K., Mohana K.N.S., Mohanan A., Madhusudhana A.M., Evaluation of anti-corrosion performance of modified gelatin-graphene oxide nanocomposite dispersed

in epoxy coating on mild steel in saline media, *Colloids and Surfaces A: Physicochemical and Engineering Aspects*, **587**: 124341, 2020, doi: 10.1016/j.colsurfa.2019.124341.

29. Khodair Z.T., Khadom A.A., Jasim H.A., Corrosion protection of mild steel in different aqueous media via epoxy/nanomaterial coating: preparation, characterization and mathematical views, *Journal of Materials Research and Technology*, **8**(1): 424–435, 2019, doi: 10.1016/j.jmrt.2018.03.003.

30. Tang F., Bao Y., Chen Y., Tang Y., Chen G., Impact and corrosion resistances of duplex epoxy/enamel coated plates, *Construction and Building Materials*, **112**: 7–18, 2016, doi: 10.1016/j.conbuildmat.2016.02.170.

31. Wang Y.Q., Kong G., Che C.S., Zhang B., Inhibitive effect of sodium molybdate on the corrosion behavior of galvanized steel in simulated concrete pore solution, *Construction and Building Materials*, **162**: 383–392, 2018, doi: 10.1016/j.conbuildmat.2017.12.035.

32. Pokorný P., Tej P., Kouřil M., Evaluation of the impact of corrosion of hot-dip galvanized reinforcement on bond strength with concrete – a review, *Construction and Building Materials*, **132**: 271–289, 2017, doi: 10.1016/j.conbuildmat.2016.11.096.

33. Singh D.D.N., Ghosh R., Electroless nickel–phosphorus coatings to protect steel reinforcement bars from chloride induced corrosion, *Surface and Coatings Technology*, **201**(1–2): 90–101, 2006, doi: 10.1016/j.surfcoat.2005.10.045.

34. Mukhopadhyay A., Sahoo S., Corrosion protection of reinforcement steel rebars by the application of electroless nickel coatings, *Engineering Research Express*, **1**(1): 015021, 2019, doi: 10.1088/2631-8695/ab35f0.

35. Mukhopadhyay A., Sahoo S., Improving corrosion resistance of reinforcement steel rebars exposed to sulphate attack by the use of electroless nickel coatings, *European Journal of Environmental and Civil Engineering* (in press), 2021, doi: 10.1080/19648189.2021.1886177.

36. Karimzadeh A., Rouhaghdam A.S., Aliofkhazraei M., Miresmaeili R., Sliding wear behavior of Ni-Co-P multilayer coatings electrodeposited by pulse reverse method, *Tribology International*, **141**: 105914, 2020, doi: 10.1016/j.triboint.2019.105914.

37. Allahyarzadeh M.H., Aliofkhazraei M., Rezvanian A.R., Torabinejad V., Rouhaghdam A.S., Ni-W electrodeposited coatings: characterization, properties and applications, *Surface and Coatings Technology*, **307**, Part A: 978–1010, 2016, doi: 10.1016/j.surfcoat.2016.09.052.

38. Loto C.A., Electroless nickel plating – a review, *Silicon*, **8**(2): 177–186, 2016.

39. Sahoo P., Das S.K., Tribology of electroless nickel coatings – a review, *Materials Design*, **32**(4): 1760–1775, 2011, doi: 10.1016/j.matdes.2010.11.013.

40. Ribeiro D.V., Abrantes J.C.C., Application of electrochemical impedance spectroscopy (EIS) to monitor the corrosion of reinforced concrete: a new approach, *Construction and Building Materials*, **111**: 98–104, 2016, doi: 10.1016/j.conbuildmat.2016.02.047.

41. Bureau of Indian Standards, https://bis.gov.in/qazwsx/sti/STI1786PP6.pdf (accessed March 15, 2021).

42. Duari S., Mukhopadhyay A., Barman T.K., Sahoo P., Investigation of friction and wear properties of electroless Ni-P-Cu coating under dry condition, *Journal of Molecular and Engineering Materials*, **4**(04): 1640013, 2016, doi: 10.1142/S225123731640013X.

43. Achuthamenon Sylajakumari P., Ramakrishnasamy R., Palaniappan G., Taguchi grey relational analysis for multi-response optimization of wear in co-continuous composite, *Materials*, **11**(9): 1743, 2018, doi: 10.3390/ma11091743.

44. Prusty J.K., Pradhan B., Multi-response optimization using Taguchi-Grey relational analysis for composition of fly ash-ground granulated blast furnace slag based geopolymer concrete, *Construction and Building Materials*, **241**: 118049, 2020, doi: 10.1016/j.conbuildmat.2020.118049.

45. Prakash K.S., Gopal P.M., Karthik S., Multi-objective optimization using Taguchi based grey relational analysis in turning of rock dust reinforced aluminum MMC, *Measurement*, **157**: 107664, 2020, doi: 10.1016/j.measurement.2020.107664.

46. Das S.K., Sahoo P., Tribological characteristics of electroless Ni-B coating and optimization of coating parameters using Taguchi based grey relational analysis, *Materials Design*, **32**(4): 2228–2238, 2011, doi: 10.1016/j.matdes.2010.11.028.

47. Mukhopadhyay A., Sahoo S., Corrosion performance of steel rebars by application of electroless Ni-P-W coating – an optimization approach using grey relational analysis, *FME Transactions*, **49**: 445–455, 2021, https://www.mas.bg.ac.rs/_media/istrazivanje/fme/vol49/2/20_s._sahoo_et_al.pdf.

48. Liu J., Wang X., Tian Z., Yuan M., Ma X., Effect of copper content on the properties of electroless Ni-Cu-P coatings prepared on magnesium alloys, *Applied Surface Science*, **356**: 289–293, 2015, doi: 10.1016/j.apsusc.2015.08.072.

49. Liu Y., Zhao Q., Study of electroless Ni-Cu-P coatings and their anti-corrosion properties, *Applied Surface Science*, **228**(1–4): 57–62, 2004, doi: 10.1016/j.apsusc.2003.12.031.

50. Chen J., Zou Y., Matsuda K., Zhao G., Effect of Cu addition on the microstructure, thermal stability, and corrosion resistance of Ni-P amorphous coating, *Materials Letters*, **191**: 214–217, 2017, doi: 10.1016/j.matlet.2016.12.059.

51. Roy S., Sahoo P., An experimental approach for optimizing coating parameters of electroless Ni-P-Cu coating using artificial bee colony algorithm, *International Scholarly Research Notices*, **2014**: Article ID 976869, 12 pages, 2014, doi: 10.1155/2014/976869.

52. Ankita S., Singh A.K., Corrosion and wear resistance study of Ni-P and Ni-P-PTFE nanocomposite coatings, *Central European Journal of Engineering*, **1**(3): 234–243, 2011, doi: 10.2478/s13531-011-0023-8.

Received May 7, 2021; accepted version July 15, 2021.